Electrochimica Acta 106 (2013) 483–493

Contents lists available at SciVerse ScienceDirect

Electrochimica Acta

journal homepage: www.elsevier.com/locate/electacta

Insights about the irreversible capacity of $LiNi_{0.5}Mn_{1.5}O_4$ cathode materials in lithium batteries

Sergio Brutti [a,**], Giorgia Greco [b], Priscilla Reale [b], Stefania Panero [b,*]

[a] Dipartimento di Scienze, Università della Basilicata, Via Nazario Sauro 85, 85100 Potenza, Italy
[b] Dipartimento di Chimica, Sapienza Università di Roma, P.le Aldo Moro 5, 00185 Roma, Italy

ARTICLE INFO

Article history:
Received 3 October 2012
Received in revised form 16 May 2013
Accepted 22 May 2013
Available online 3 June 2013

Keywords:
Li-ion batteries
Cathodes
Irreversible capacity
Electrolyte decomposition

ABSTRACT

The accumulation of irreversible capacity in the first cycle and upon cycling has been studied for $LiNi_{0.5}Mn_{1.5}O_4$-based cathodes (LNMO), bare and coated with ZnO. Materials have been synthesized at 800 °C and characterized by X-ray diffraction and transmission electron microscopy (TEM). The precipitation of a continuous ZnO film on the surface of LNMO has been highlighted by TEM. Galvanostatic cycling at room temperature and at 60 °C, linear sweep voltammetry (LSV), impedance spectroscopy and TEM techniques have been used to investigate the materials and the irreversible capacity accumulation upon cycling.

Our study confirms that continuous parasitic processes occur upon cycling beyond the first charge/discharge. Anodic LSV test shows that side oxidation processes start on the surface of a LNMO electrode at potential slightly above the Ni^{2+}/Ni^{4+} redox couple. At the end of charge an uniform and continuous thin film (3–4 nm) forms of on the bare LNMO. This film likely modifies upon cycling and it is apparently unable to passivate the LNMO surface preventing further decompositions. On the contrary the material coated with ZnO shows rough surfaces without large morphological alteration upon charge and cycling. The ZnO coating confirms its ability to mitigate the irreversible charge consumption.

1. Introduction

The development of new cathode materials for Li-ion cells is one of the key issues to develop batteries with improved performances, suitable for automotive applications. $LiCoO_2$ is the typical used cathode material in commercial lithium-ion batteries. However lithium cobaltites suffer economic and environmental drawbacks: intense research efforts are spent worldwide to find substitutes. Among these the $LiN_{0.5}Mn_{1.5}O_4$ spinel (LNMO) has been intensively studied in the last decade mainly because of its high working voltage (>4.7 V) and improved environmental compatibility [1].

LNMO exploits the redox couple Ni^{2+}/Ni^{4+} to provide one Li atom per formula unit and a theoretical specific capacity of 146.5 mAh g^{-1}. Its oxidation occurs in a stable voltage plateau around 4.75–4.85 V vs. Li^+/Li.

In the first electrochemical Li de-insertion/insertion LNMO suffers irreversible capacity losses: in the following cycles, at room temperature, it shows high reversibility and stable cycling performances, from low to high current rates. On the contrary above 50 °C, LNMO suffers a quick deterioration of the performances due to the growth of parasitic reactions with the electrolyte [2].

The occurrence of electrolyte decomposition upon cycling is unavoidable due to the high working voltage of LNMO, i.e. 4.75–4.85 V vs. Li^+/Li, at the upper limit of the thermodynamic stability window of any organic carbonate currently adopted in Li-cells. As a consequence LNMO supplies more than one nominal lithium per formula unit (e.g. [3]) at low rates, going beyond the theoretical capacity. This results in a poor coulombic efficiency in the first complete cycle [4]. These drawbacks limit the adoption of LNMO in Li-cells and require developing specific strategies to suppress the parasitic reactions.

The investigation of the capacity fading in LNMO electrodes has been addressed recently by various authors. In a series of papers Aurbach and co-workers [5–7] observe that LNMO nanoparticles are much more reactive towards $LiPF_6$-based electrolytes compared to microsized LNMO materials (see also Ref. [8]). Apparently the chemistry of the interaction of LNMO with electrolytes involves a nucleophilic reaction between the ethylene carbonate molecule from the electrolyte and the negatively charge oxygen on the surface of LNMO particles. Such reaction occurs in parallel with the oxidation of LNMO and may lead to the precipitation of organic carbonates, alkoxydes and polycarbonates. The formation of these carbonaceous by-products has been confirmed by Yang and co-workers that observed the formation of poly-ethylencarbonate on

* Corresponding author. Tel.: +39 06 49913703; fax: +39 06 491769.
** Corresponding author.
E-mail addresses: sergio.brutti@unibas.it, sergio.brutti@uniroma1.it (S. Brutti), stefania.panero@uniroma1.it (S. Panero).

0013-4686/$ – see front matter © 2013 Elsevier Ltd. All rights reserved.
http://dx.doi.org/10.1016/j.electacta.2013.05.111

LNMO after prolonged potentiostatic holds at 5.0 and 5.3 V [9]. Also the precipitation of fluorine-containing species, i.e. LiF, $Li_xMO_yF_z$ and MnF_2, on the LNMO surface has been observed or speculated [5,10–12]. In particular the smooth capacity fading in prolonged cycling at room temperature seems to be related to accumulation of LiF and the concomitant thickening of the surface films [10,13]. These parasitic reactions are likely promoted by the traces of HF unavoidably present in any electrolyte. In fact HF acts as scavenging agent that leads to the dissolution of Mn^{2+} ions from the LNMO surface through the following process [7,14]:

$$4LiNi_{0.5}Mn_{1.5}O_4 + 8HF \rightarrow \lambda\text{-}MnO_2 + MnF_2 + NiF_2 + 4LiF + 4H_2O + 2Ni_{0.5}Mn_{1.5}O_4 \quad (R1)$$

At temperatures above 50 °C all these parasitic processes are enhanced [14] thus leading to the quick deterioration of the performances of LNMO in lithium cells.

The deposition of a ZnO coating apparently limits the Mn^{2+} loss by reducing the amount of free HF in the electrolyte, and stabilizes the cycling above room temperature, as discussed by Sun and co-workers [15,16] and recently re-examined by Arrebola et al. [4]. Moreover, the ZnO coating also mitigates the deposition on the surface of the LNMO of carbonaceous species due to the decomposition of the electrolyte at high voltages [15,16]. Aurbach et al. [7] studied in detail the effect of coating LNMO with ZnO and MgO nanoparticles. Apparently these coatings protect the LNMO surface from the acidic molecules in the standard electrolyte solutions based on $LiPF_6$. This effect reduces the dissolution of Mn and Ni ions into the electrolyte thus mitigating the charge losses. Furthermore, Aurbach et al. [7] infer that ZnO and MgO can also easily convert to the corresponding insoluble difluorides by direct reaction with the HF, by releasing water molecules ($MO + 2HF = MF_2 + H_2O$), thus reducing the amount of free H^+ in the electrolyte. This effect can limit the above-mentioned H^+-catalyzed reaction (R1). On the other hand as ZnO and MgO coating materials are highly hygroscopic, water can hydrate their surfaces: such hydration can de-activate water molecules and can inhibit the further formation of HF through the reaction

$$LiPF_6 + H_2O = POF_3 + 2HF$$

In this paper insights about the irreversible capacity loss in the first cycle for LNMO are reported in comparison to the same LNMO material coated with ZnO. The goal is to investigate the decomposition of the electrolyte on the surface of LNMO at high voltage in standard galvanostatic experiments at room temperature, by electrochemical tests and transmission electron microscopy.

2. Experimental details

LNMO has been synthesized by co-precipitation from an aqueous solution of the Mn^{2+}, Ni^{2+} and Li^+ nitrates [17]. Stoichiometric amounts of the corresponding nitrates have been dissolved in few millilitres of water and the solution was kept at 50 °C under vigorous stirring until complete H_2O evaporation. The mixed nitrate has been transferred in an alumina crucible and fired in air at 800 °C for 12 h. The resulting powder has been hand grinded and newly annealed at 850 °C for 12 h followed by controlled cooling to room temperature at 1 °C/min.

The ZnO coating has been obtained by suspending the LNMO powder in few millilitres of water by vigorous stirring. A stoichiometric amount of Zn^{2+} acetate (corresponding to a final ratio of 1.5 wt% of ZnO) has been added to the aqueous suspension and the resulting solution has been heated and kept under stirring at 40–50 °C for few hours, until complete H_2O evaporation. The resulting composite powder has been annealed in air at 500 °C for 30 min with a heating/cooling rate of 1 °C/min [18].

The materials have been characterized by X-ray diffraction (XRD), scanning electron microscopy (SEM) with energy dispersive spectroscopy (EDS), transmission electron microscopy (TEM) and elemental analysis by inductively coupled plasma atomic absorption (ICP-AA).

The XRD experiments have been carried out using a Rigaku X-ray Ultima$^+$ diffractometer equipped with a Cu Kα source and a graphite monocromator for the diffracted beam. SEM images have been obtained by an Oxford Instruments LEO 1450VP. The EDS analyses have been performed using an INCA X-sight Oxford Instruments apparatus. The TEM micrographies have been obtained by a JEOL JEM 2011 HR TEM instrument. The Fourier Transform Infrared (FTIR) spectroscopy tests have been carried out by a Bruker Alpha FTIR in transmission using KBr pellets: the pellets preparation and FTIR experiments have been carried out in an Ar-filled glove box.

The electrochemical tests have been carried out on casted electrodes. The cathode films have been deposited on an aluminium foil by doctor-blading a slurry composed of 80% of the active material (AM), 10% of poly-vinyl-difluoride (PVDF 6020 Solvay Solef) and 10% of SuperP carbon. The mass loading over the aluminium foil is approximately 2.5 mg cm^{-2}. The electrochemical performances of the active materials have been recorded on cells assembled using a working electrode prepared as described above, combined with a lithium counter electrode. The adopted electrolyte is a 1 M $LiPF_6$ solution in an ethylene carbonate–dimethyl carbonate mixture, EC:DMC 1:1 (LP30, Merck Battery Grade), soaked on a Whatman™ separator. Cells have been assembled in an MBraun-type dry box with moisture and oxygen levels below 1 ppm. The galvanostatic cyclings (CG) have been performed in two electrodes cell. The CG tests have been carried out at various specific currents, normalized for the active materials weight, within a 3.5–5.0 V limits unless differently indicated, using a Maccor Series 4000 Battery Test System. The materials for ex situ TEM analysis have been obtained by deassembling the cells and washing the electrodes in DMC and THF in glove box under Ar. Impedance spectroscopy experiments have been carried out on three electrodes cells with a lithium reference electrode, using the Solartron Analytical Modulab apparatus. All EIS experiments have been carried out on electrodes with identical mass loads per square centimetre and thicknesses in a frequency range 100 kHz–10 mHz with a voltage signal of 5 mV.

3. Results and discussion

3.1. Materials characterization and electrochemical performances in lithium cells

As expected the pristine and the ZnO coated LNMO materials show identical XRD patterns (see Fig. 1 of Ref. [18]): apparently diffraction is unable to detect the precipitation of zinc oxide at such small ZnO concentrations, as already pointed out by Sun et al. [2], Arrebola et al. [4] and us in a previous publication [18]. On the contrary electron microscopy is able to detect the ZnO coating: Fig. 1a and b shows HRTEM (high resolution TEM) images of bare and coated LNMO. The corresponding three-dimensional (3D) reconstructions obtained by the ImageJ software are presented in Fig. 1c and d [19,20]. A fast Fourier Transform (FFT) analysis of the HRTEM of the uncoated material is shown as an inset in Fig. 1a. The reciprocal lattice shown in the inset of Fig. 1a can be indexed with an fcc structure with a cell constant of 8.0(3) Å corresponding to the LNMO spinel lattice [17]: it is in agreement within the errors with the 8.19(4) Å lattice parameter derived from the XRD pattern. The linear greyscale profile calculated on the outer layer of particle shown in the HRTEM image of the coated sample is shown the inset of Fig. 1b. It is possible to estimate a length periodicity in the

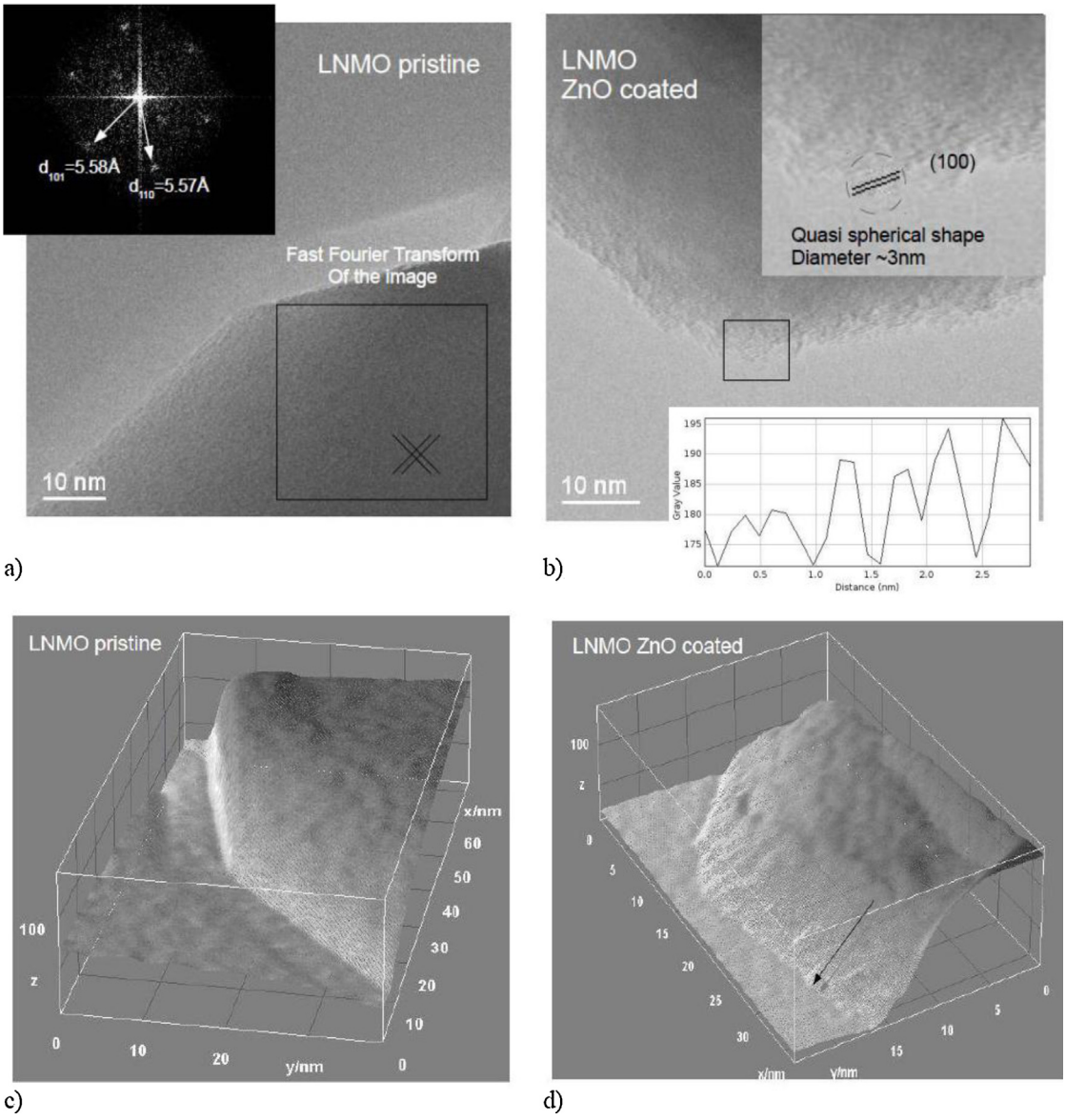

Fig. 1. (a) HRTEM image of the LNMO spinel pristine material. In the inset the fast Fourier Transform (FFT) of the HRTEM image shows lattice reflections (the cross lines in the main 1 figure are only indication marks to highlight the area where the FFT has been calculated); (b) HRTEM image of the LNMO spinel ZnO coated material, cross-sectional line profile taken from the ZnO coating. (c) and (d) Three-dimensional reconstructions from the HRTEM images.

greyscale oscillations of ~4.8 Å, a value that is in excellent agreement with to the lattice parameter of the ZnO zincoblende cubic structure [21]. Turning to the 3D images (Fig. 1c and d), there is an evident alteration of the surface of the coated particles compared to the bare LNMO. TEM images suggest the formation of a continuous rough film, constituted by ZnO, precipitated on the surface of the LNMO particles with mean thickness of 3–5 nm.

The voltage profiles of the uncoated and coated materials in lithium cells are shown in Fig. 2. The two curves show very similar shapes. Three main effects are induced by the ZnO coating: (i) a 15% reduction of the charge capacity (148 vs. 127 mAh g^{-1} for the bare and the coated materials, respectively); (ii) a 30% decrease of the irreversible capacity loss in the first Li^+ de-insertion/insertion cycle (35 vs. 24 mAh g^{-1} for the bare and the coated materials, respectively); (iii) a slight increase in the potential hysteresis between charge and discharge (70 mV vs. 100 mV for the bare and the coated materials, respectively). These experimental evidences can be explained by considering the role played by the ZnO coating as HF trap [7,15,16]. In fact the decrease of the unavoidable traces of free HF in the electrolyte is expected to mitigate the LNMO surface scavenging thus limiting the occurrence of further parasitic reactions. It is to be noted that the increased voltage hysteresis between charge and discharge is likely due to the presence of the ZnO layer. In fact it probably negatively affects the electron mobility within the electrode and the lithium ion diffusion across the electrolyte/electrode interface.

The two bare and coated materials show comparable performances in GC at room temperature as shown in Fig. 3. The coated material shows a smaller cumulative irreversible capacity loss upon cycling (i.e. the sum over cycles of the difference between the charge and discharge capacity) only partially counterbalanced by a slight decrease of the reversible specific capacity.

At 60 °C the bare material suffers a diverging cumulative irreversible capacity loss upon cycling and a continuous fading of the cycled specific capacities. After 80–90 cycles the performances at 60 °C of the bare LNMO electrodes dramatically drop (result checked in duplicate) similarly to what observed by Sun and co-workers [2,15,16]. As expected the parasitic reactions occur

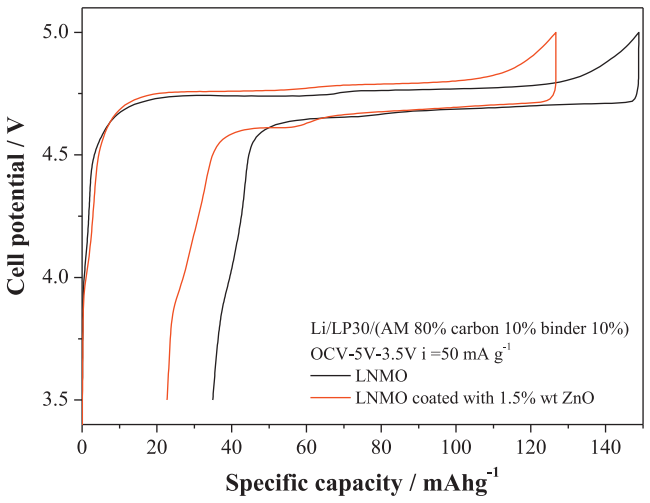

Fig. 2. Galvanostatic voltage profiles (first cycle) of the LNMO material bare and coated with ZnO.

faster at higher temperatures thus leading to a steeper trend in the cumulative irreversible capacity. The bare LNMO material suffers a cumulative irreversible capacity loss larger than 100 mAh g^{-1} at cycle 13 at room temperature to be compared to cycle 8 for the GC at 60 °C. On the contrary the ZnO coated material shows a remarkable stability upon cycling with minor losses in the specific capacity and a smaller cumulative irreversible capacity loss in comparison with the bare material. In fact the coated material reaches a cumulative irreversible capacity loss that exceed 100 mAh g^{-1} at cycle 36 (room temperature) and at cycle 32 (60 °C).

On passing, it is interesting to observe that the galvanostatic cycling at 55 °C of the uncoated LNMO synthesized by Sun et al. [15] shows an immediate dramatic loss in the specific capacity after the third cycle, with a capacity retention after 50 cycles of about 25%. On the contrary Arrebola et al. [4] report stable performances for the bare material at 50 °C. However the comparison is biased not only by the small differences in the temperatures but mainly by the different anodic voltage cut-offs, i.e. 5.3 V and 5 V for Sun et al. and Arrebola et al., respectively, to be compared to the 5 V cut-off used in our tests. In fact an anodic polarization beyond 5 V, well above the working potential of the LNMO material, is expected to strongly enhance any parasitic reactions on the surface of the electrode and to facilitate its failure.

In summary, at temperatures above 25 °C, parasitic reactions occur continuously upon cycling on the surface of LNMO-based materials. The growth of a ZnO film on the surface of the active material is capable to mitigate such capacity losses at room temperature as well as at 60 °C.

3.2. Impedance spectroscopy tests upon cycling

The EIS spectra of the charged (at 5 V vs. Li^+/Li) and discharges electrodes (at 3.5 V vs. Li^+/Li) are presented in Fig. 4 for both the bare and the coated materials.

The impedance of the electrodes in their discharged state is always larger than in the charged state in agreement with Amatucci et al. [23] and Davidson et al. [10]. This phenomenon is generally ascribed to the higher resistivity of manganite-based electrodes in their lithiated state compared to the de-lithiated one [22,23] due to the smaller ion mobility and electronic conductivity.

The equivalent circuit for this class of material electrodes (i.e. $LiMn_2O_4$ manganites) has been discussed and proposed by Aurbach and co-workers [22]. It consists of the resistance of the solution R_s, in series with a block consisting of the resistance of the electrode surface, R_f, in parallel with is capacity, C_f. This section is in series with another similar block consisting of the charge-transfer resistance. R_{ct}, in parallel with the double layer capacitance, C_{dl}. A final Warburg impedance at low frequency, W, is found in series to all these elements and is likely related to the solid state Li^+ ion diffusion [10,22]. The final equivalent circuit is summarized by the following string: $R_s(R_fC_f)(R_{ct}C_{dl})W$.

The first (R_fC_f) block fits the first part of the EIS spectra, i.e. the high to medium frequency semicircle, and can be attributed to the migration of Li^+ ions from the electrolyte through the surface films of the active material particles. In this view this section of the EIS spectra gives direct insights about the precipitation and growth of a passivation film, its properties and changes upon cycling.

The EIS spectra shown in Fig. 4 for both charged and discharge states show a first semi-circle in the high-medium frequency range and a second semi-circle, very large and not completed, in the medium-low frequency range. The first semi-circles are fitted by the (R_fC_f) block of the above discussed equivalent circuit. The C_f capacitance values ($C_f \sim 10^{-6}$–10^{-5} F) confirm in all cases that these semi-circles are related to a surface layer formed on the active material. This surface layer is probably a passivation film constituted by the electrolyte decomposition products precipitated on the LNMO particles and in the case of the coated material above the ZnO coating. The plots of the fitted passivation film resistances, R_f, are shown in Fig. 3.

It is important to underline that, in all cases, the passivation film resistances (R_f) are for both the charged and the discharged states larger in the case of the bare LNMO electrode compared to the coated one.

The bare material shows for the charged states a rapid increase in the passivation film resistance in the firsts 3 cycles followed by a smooth increasing trend. The coated material shows in the first cycle a passivation film resistance very similar to the bare LNMO: however in the following cycles it shows only a slightly positive slope without abrupt changes.

In the discharged states the passivation film resistance for the bare material shows a constant increasing trend upon cycling. On the contrary the passivation film resistance of the coated material oscillates upon cycling without showing a monotonic increasing trend.

The EIS results agree with the trends of the cumulative irreversible capacity in CGs at room temperature. In the case of the bare LNMO material the increase of the passivation film resistance upon cycling occurs in parallel with the accumulation of irreversible capacity. Apparently these losses correspond to the precipitation of by-products on the surface of the LNMO material, thus leading to a probable thickening of the passivation film or its densification.

Turning to the coated material, apparently the EIS results highlight a smaller resistance of the passivation film as well as a smaller increasing trend upon cycling in comparison with the bare LNMO. The impedance data confirm the ability of the ZnO coating to limit the accumulation of insoluble decomposition by-products on the electrode surface.

3.3. Analysis of the irreversible capacity loss in the first electrochemical Li de-insertion/insertion cycle: linear sweep voltammetry and ex situ TEM analysis

Linear sweep voltammetry (LSV) tests have been carried out for the bare and coated materials from the OCV (open circuit voltage) to 6 V vs. Li^+/Li. The results are shown in Fig. 5.

Both materials show a current peak centred at about 4.8 V vs. Li^+/Li due to the lithium removal and the concomitant oxidation of the Ni^{2+} ions in the LNMO lattice. The peak for the coated material is broader and asymmetric compared to the bare LNMO.

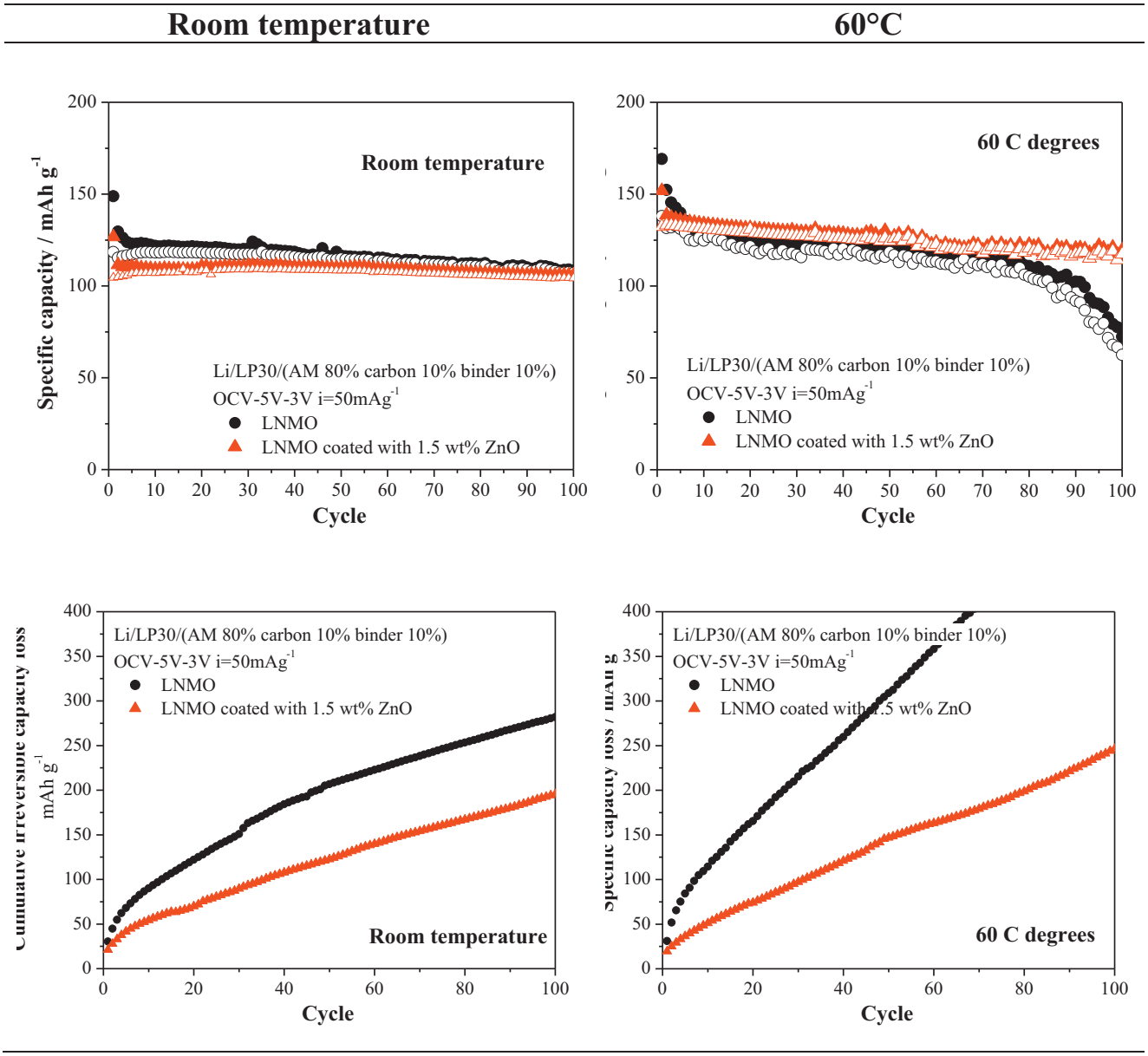

Fig. 3. (a) and (b) Performances in galvanostatic tests of the bare and the ZnO coated LNMO materials at room temperature and at 60 °C and (c) and (d) corresponding cumulative irreversible capacity loss plots.

At about 5 V this process overlaps with another minor electroactive reaction in both cases. In the case of the ZnO coated material, this second anodic peak is broader: it is also shifted at higher potential compared to the bare material, i.e. $V > 4.9$ V and 5 V vs. Li^+/Li, for the bare and the coated LNMO, respectively. Both these processes cannot be ascribed to a reversible oxidation of LNMO: more likely they are related to the oxidation of some electrolyte components. Such decompositions may lead to the precipitation of insoluble organic molecules (e.g. polyethers and organic carbonates $ROCO_2M$) that may accumulate on the electrode surface, as reported in literature [10,13].

Above 5.5 V vs. Li^+/Li in both cases massive decomposition reactions occur. These voltammetric peaks can be attributed to the evolution of CO_2 at the cathode side, as well as the production of many other gaseous by-products from the oxidation of the electrolyte solvent molecules (CO_2, CO, H_2, CH_4, C_2H_6 and C_2H_4) [24].

The linear sweep voltammetry tests suggest that on the surface of a LNMO electrode a first parasitic oxidation process starts at potential similar to the Ni^{2+}/Ni^{4+} redox couple. The ZnO coating is apparently able to broaden this process on a larger voltage range and to shift upwards the peak current for this undesired reaction, beyond 5 V vs Li^+/Li. As already mentioned this process can be attributed to a parasitic oxidation of an electrolyte components. One can speculate that the upward shift of the peak potential above 5.0 V due to the ZnO coating may result from a barrier to the electron transfer, from the electrolyte to the electrode, due to the insulating ZnO layer.

The ex situ TEM images of the bare and coated materials charged at 4.7 (before the working voltage) and at 5 V vs. Li^+/Li (end of charge) are shown in Fig. 6. The bare material surface shows the precipitation of a continuous surface film at 5.0 V as well as 4.7 V vs. Li^+/Li, well before the onset of the parasitic oxidation process

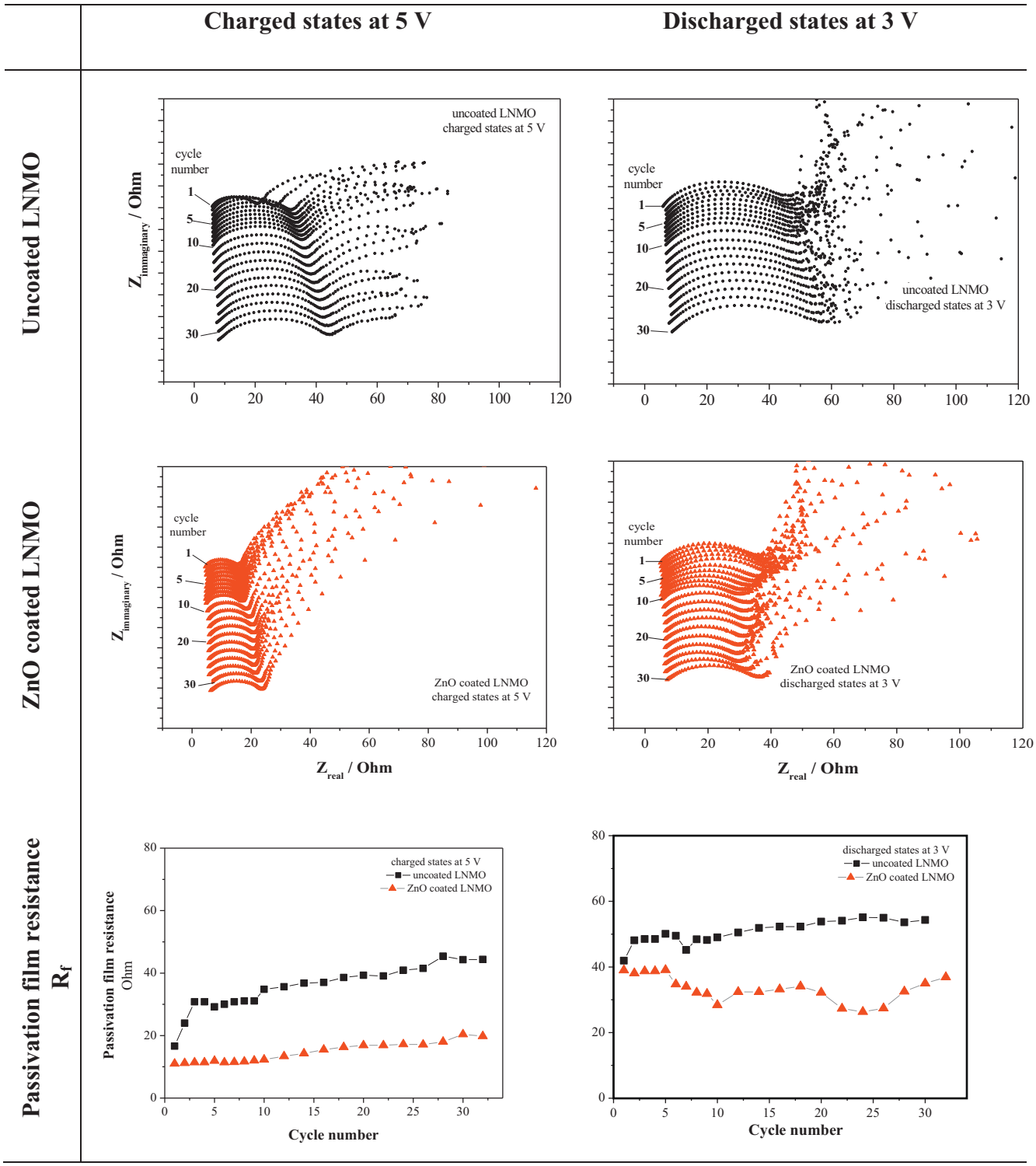

Fig. 4. EIS spectra in charged and discharged states upon cycling of the bare and ZnO coated LNMO materials. Cells have been cycled at 50 mAh g^{-1} in the voltage range 5–3.5 V vs. Li^+/Li.

observed in the LSV. The thickness of the passivation film is about 3–4 nm and apparently covers uniformly the surface of the LNMO lattice. The morphology of this surface film is very similar to the MnF_2 layer experimentally observed by TEM by Aurbach and co-workers [7]. This surface layer is likely due to the abovementioned reaction (R1) that is activated and fed by the unavoidable HF traces in the electrolyte [7,14]. On passing it is important to remind that the formation of such thin and continuous film on the surface of the bare material does not prevent further accumulation of irreversible capacity losses upon cycling (see previous section). Apparently this film is unable to passivate the LNMO surface.

A surface film on the LNMO particles is also observed in the case of the ZnO coated material. It is morphologically very different from that observed on the bare LNMO: it is not uniform and it is remarkably rough. From the morphological point of view this film is very similar to pristine ZnO coating (see Fig. 1). Owing to

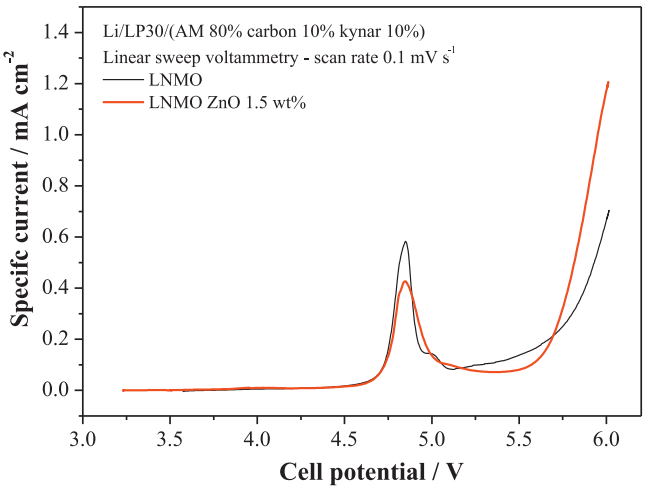

Fig. 5. Anodic linear sweep voltammetry tests of the bare and the ZnO coated LNMO materials.

this it is very difficult to discriminate between the original ZnO coating and the further SEI layer formed on it. The thickness of the film observed on the ZnO coated LNMO particles charged at 4.7 and 5.0 V vs. Li^+/Li ranges between 5 and 8 nm whereas the pristine ZnO coating is about 3–5 nm thick (see Fig. 1). The apparent thickening of the film would suggest the accumulation of limited amounts of amorphous-like substances on the ZnO coating. However the precipitation of these electrolyte decomposition by-products does not form a continuous and uniform film.

The different morphology of the two film formed on the bare and the ZnO coated LNMO may suggest a different chemical composition. As an example, in the view of the observation by Aurbach and co-workers [7], our TEM images could suggest that the ability of ZnO to capture water and to decrease the free acidity by HF in the electrolyte (see also [7]), may limit the occurrence of the abovementioned spontaneous reaction (R1), therefore reducing the scavenging of manganese/nickel ions to form insoluble fluorides.

3.4. Analysis of the irreversible capacity loss in the first electrochemical Li de-insertion/insertion cycle: galvanostatic charge/discharge and impedance spectroscopy tests

In order to analyze more in detail the accumulation of charge losses upon charge/discharge we carried out a study of the evolution of the coulombic efficiency with the anodic voltage cut-off for both the bare and the ZnO coated material. The results are presented in Fig. 7.

The evolution of the specific capacity in charge and the irreversible capacity accumulation in the first cycle show similar trends for both materials. However, the coated material shows

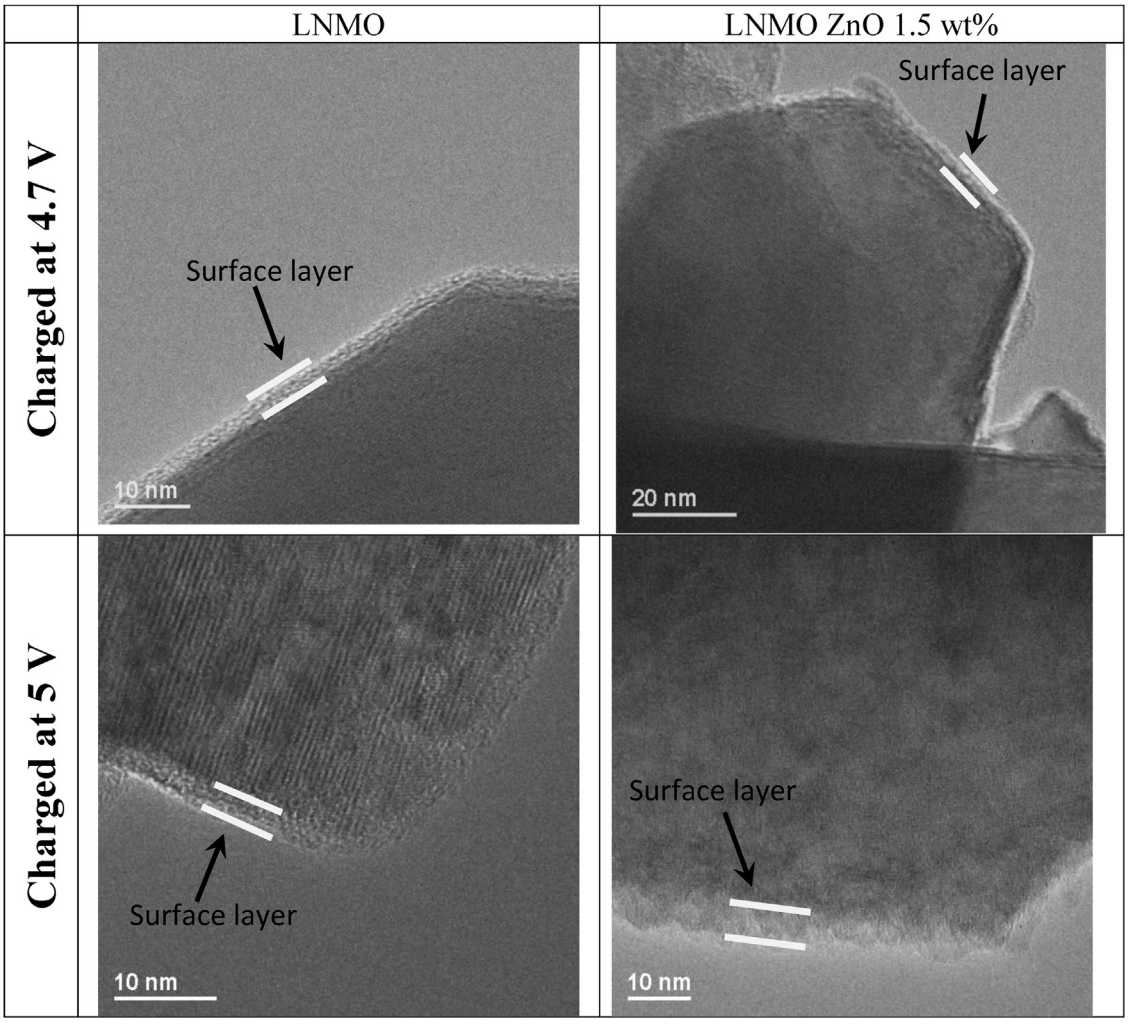

Fig. 6. Ex situ transmission electron micrographs of the bare and the ZnO coated LNMO materials charged at 4.7 and 5 V vs. Li^+/Li.

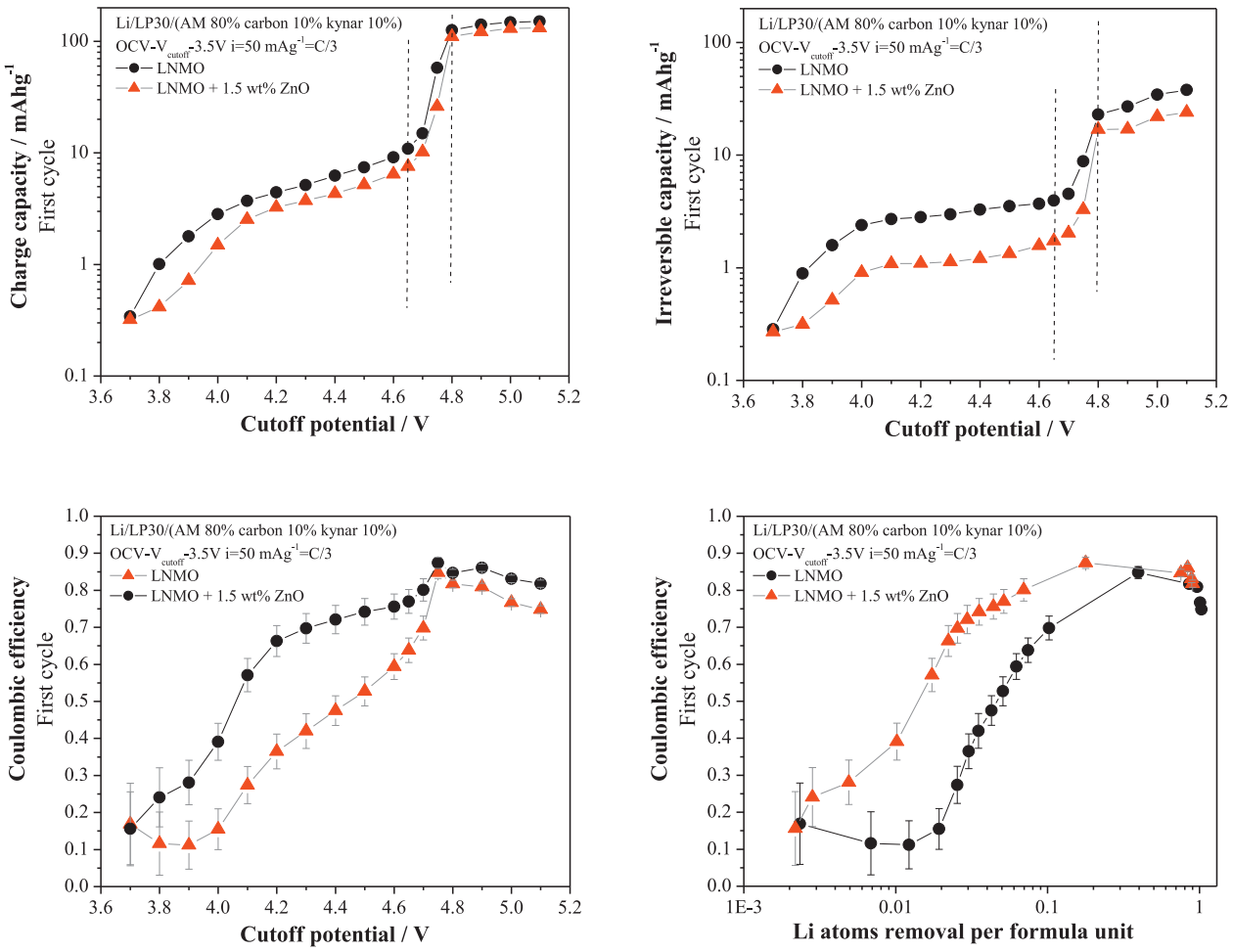

Fig. 7. Performances in galvanostatic tests at various anodic cut-off potentials of the uncoated and coated LNMO materials.

improved reversibility, i.e. smaller irreversible capacity losses and larger coulombic efficiencies, in the whole voltage cut-offs range, compared to the bare one.

It is possible to identify three voltage regions: (1) from the OCV to 4.65 V vs. Li^+/Li; (2) the intermediate range between 4.65 and 4.8 V vs. Li^+/Li and (3) potentials above 4.8 V vs. Li^+/Li. A summary of the galvanostatic performances of the bare and coated materials in the three voltage ranges is presented in Table 1.

1. At cell potential <4.65 V vs. Li^+/Li the specific capacity in charge is mainly due to the oxidation of the redox couple Mn^{3+}/Mn^{4+}. The LNMO lattice should not contain Mn^{3+} ions. However this undesired contamination is well known and is apparently unavoidable: it occurs in parallel with the precipitation of nickel oxide during the synthesis [1,18]. In this voltage range the bare material supplies a specific capacity approximately 30% larger compared to the coated material. However this larger charge capacity is due mainly to irreversible parasitic processes: in this voltage range the coulombic efficiencies for the bare material are smaller of about 20% compared to the ZnO coated material. In both cases only limited amounts of charge are irreversibly lost in this voltage range, i.e. 10 and 7% of the overall irreversible capacity loss in the first GC cycle for the bare and the ZnO coated materials, respectively.
2. In the voltage range between 4.65 and 4.8 V vs. Li^+/Li the LNMO lattice undergoes to the Ni^{2+}/Ni^{4+} oxidation process by de-intercalating two Li^+ ions per Ni^{2+}. In this voltage range the coulombic efficiencies of the two materials are very similar. The irreversible capacity losses between 4.65 and 4.8 V vs. Li^+/Li sum the main part of the inefficiency in the entire first cycle for both materials. However the coated material losses are smaller in absolute value of 20% compared to the bare one. This evidence suggests that parasitic processes occur on the surface of the bare LNMO: the ZnO coating is apparently able to mitigate these detrimental reactions.
3. The third voltage range, i.e. $4.8 < V < 5.1$ V vs. Li^+/Li, is above the working potential of the LNMO lattice. However further reversible charge is exchanged also this range, i.e. 22.1

Table 1
Specific capacity supplied in the first charge and irreversible capacity loss in function of the cut-off potential for the uncoated and the coated material.

Voltage range vs. Li^+/Li	Charge specific capacity (mAh g^{-1})		Irreversible capacity loss (mAh g^{-1})		Coulombic efficiency	
	Uncoated	Coated	Uncoated	Coated	Uncoated	Coated
$OCV < V < 4.65$	10.8	7.5	3.9	1.7	0.64	0.77
$4.65 < V < 4.8$	114.2	102.5	19.1	15.2	0.83	0.85
$4.8 < V < 5.1$	37.2	29.5	15	7.1	0.49	0.70

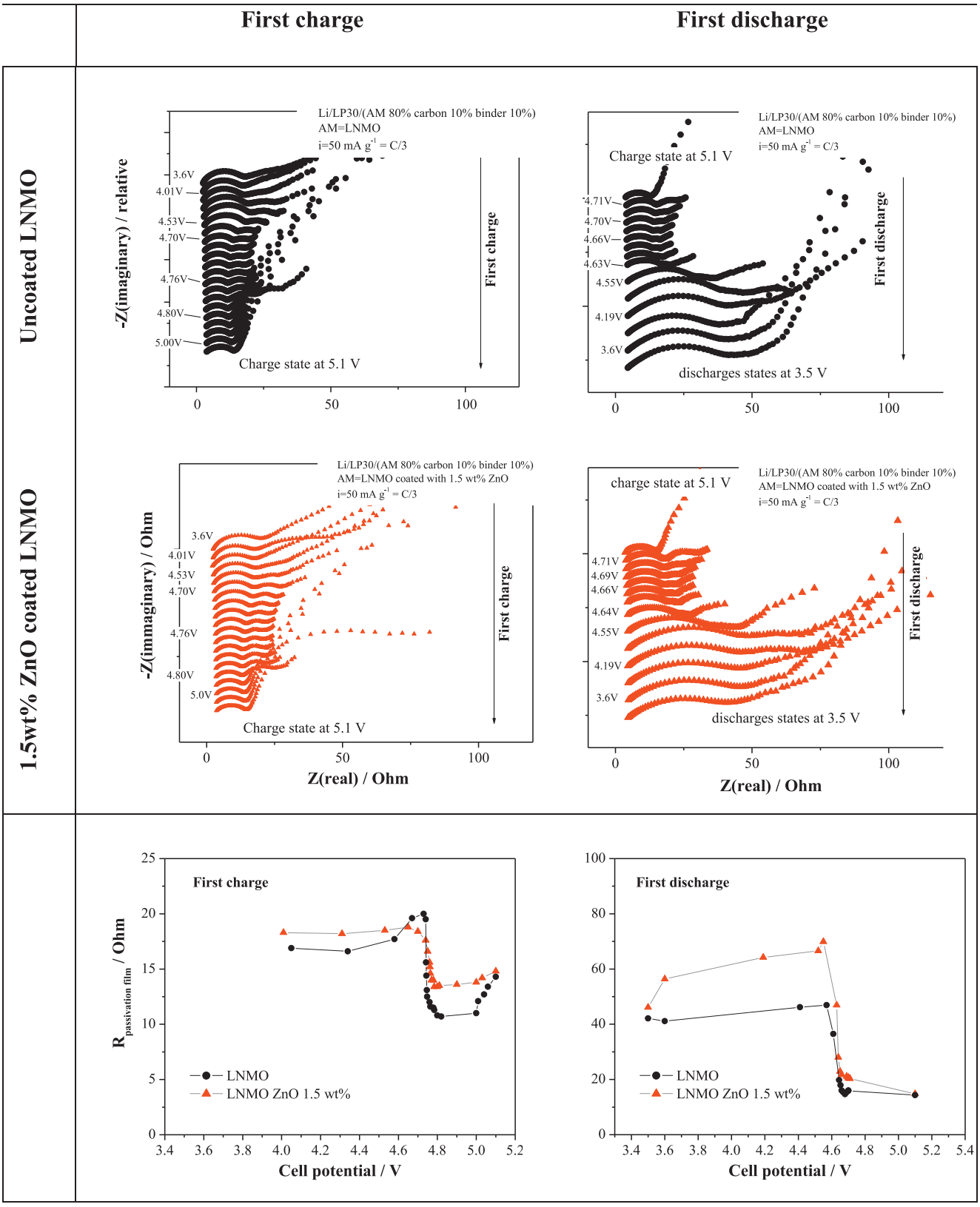

Fig. 8. EIS spectra upon first charge and discharge of the uncoated and coated LNMO materials.

and 22.4 mAh g^{-1} for the uncoated and the coated materials, respectively. This reversible capacity is probably due to kinetically limited lithium removal/insertion sites. In this voltage range the irreversible capacity suffered by the bare material doubles that observed for the ZnO coated LNMO. As a consequence, the coulombic efficiency of the bare material is largely smaller than that of the coated one. The irreversible capacity accumulated in this voltage range sum approximately 40% and

30% of the total losses suffered by the bare and the coated materials, respectively.

In order to study the modification of the electrolyte/electrode interface upon first GC cycle we carried out a detailed impedance spectroscopy experiments at various stages of charge and discharge.

The results of the two EIS experiments are presented in Fig. 8. Qualitatively the coated and the bare materials show a very similar evolution of the EIS spectra both upon charge and discharge.

As discussed above, the EIS spectra upon charge/discharge can be fitted by an equivalent circuit summarized by the string: $R_s(R_fC_f)(R_{ct}C_{dl})W$ [10,22] for both materials. Similarly to the EIS spectra reported in Fig. 4 the first semi-circle can be attributed to the formation of a surface layer whereas the second one easily is due to the charge transfer associated with the Li extraction and insertion from and into the LNMO lattice. The trends of the fitted passivation film resistances are reported in Fig. 8.

On passing it is to be noted that at the end of the first charge there is an inversion of the values of the resistances of the passivation film reported in Fig. 8 compared to Fig. 4 (first cycle). The passivation film on the bare LNMO electrodes shows at the end of charge a resistance of 18 Ω (Fig. 4) or 12 Ω (Fig. 8) whereas the ZnO coated electrodes shows 10 Ω (Fig. 4) and 14 Ω (Fig. 8). It is our opinion that, in the view of the small and similar values of the resistances of the four different cells and in the view the different charge conditions for the electrodes shown in Figs. 4 and 8, the absolute estimates of the resistance are to be considered indistinguishable. To support this opinion, although not completely rigorous, we calculated the mean values of the passivation film resistance after the first charge for both materials. The resulting values are: 15 ± 3 and 12 ± 2 Ω for the bare and the coated LNMO, respectively: they agree within the error.

The resistance of the passivation film shows slight differences between the bare and coated materials: upon Li removal (charge) three regions can be identified:

- Below 4.7 V vs. Li^+/Li: the resistance of the passivation film slightly increases in the case of the bare material whereas it is stable for the coated one.
- Between 4.7 and 4.8 V vs. Li^+/Li: the resistance of the passivation film drops of about 50% and 30% for the bare and coated materials, respectively.
- Above 4.8 V vs. Li^+/Li: the resistance of the passivation film increases for both materials with a steeper trend in the case of the bare material. The final values of the passivation film resistance are very similar for both materials.

Similarly upon Li insertion (discharge) three regions can be identified:

- Above 4.65 V vs. Li^+/Li: the resistance of the passivation film is almost constant for both materials.
- Between 4.65 and 4.55 V vs. Li^+/Li: the resistance of the passivation film drastically increases of about 180 and 250% for the bare and the coated material, respectively.
- Below 4.55 vs. Li^+/Li: the resistance of the passivation film is constant in the case of the bare material whereas it drops of about 36% for the coated one. The final values of the passivation film resistance are very similar for both materials.

The evolution of the passivation film resistance shows slight differences upon charge and discharge between the bare and the coated materials. In particular in charge the bare material shows below 4.7 and above 4.8 V vs. Li^+/Li larger increasing trends compared to the coated one. These growths occur in the same voltage ranges where it suffers the largest irreversible capacity losses in the CG tests (see Fig. 6 and Table 1). The parallel occurrence of these two effects suggests a possible increase of the thickness of the passivation film, or its densification, due to the accumulation of by-products from the parasitic oxidation of the electrolyte.

The large drops in the film resistance observed for both materials between 4.7 and 4.8 V are less easily understandable: possible explanations may involve the formation of cracks or the modification of the surface layer properties. Cracks may expose unprotected LNMO surface directly to the electrolyte, thus (a) boosting the lithium ions mobility through the electrolyte/electrode interface and (b) activating further parasitic oxidations of the electrolyte.

On the other hand the reaction mechanism of LNMO is known to have two topotactic two-phase reactions: (1) in the range Li = 1 to Li = 0.5 from cubic (a = 8.19 A) to cubic lattice (a = 8.09 A) and (2) in the range Li = 0.5 to Li = 0 from cubic (1 = 8.09 A) to cubic (a = 7.99 A) cell [1]. The volume shrinking upon lithium removal is approximately −7% and it is fully recovered upon lithium insertion. Such moderate volume variation is unlikely to be responsible of massive fractures on the surface layer. This speculation is apparently supported by the TEM data shown in Fig. 6. The ex situ TEM pictures of the bare LNMO electrodes at the end of charge show a compact and continuous thin film on the surface of the crystal particles. As already mentioned this morphology reminds that observed by Aurbach and co-workers [7]. Moreover, the morphology of this film does not apparently alter upon charge (before and after the main voltage plateau: 4.7 and 5.0 V vs. Li^+/Li, respectively).

As a consequence the abrupt variation of the resistance of the passivation layer observed in the EIS experiments cannot be easily related to the occurrence of cracks in the surface layer. More likely the film composition and density modifies upon lithium extraction from the LNMO lattice improving the lithium conductivity through this interphase.

Turning to the coated material, the evolution of its surface film resistance in the first cycle is qualitatively similar compared to the bare one. This experimental evidence suggests that, although the morphology and the composition of the surface films formed upon first charge on the bare and coated LNMO particles are different, the fundamental chemistry is similar in both cases. Apparently the ZnO coating does not alter drastically the overall picture: upon charge the ZnO coating mitigates the changes in the passivation film resistance whereas in discharge it favours the formation of a more resistive film at the end of the Li^+ insertion.

4. Conclusions

A study of the accumulation of irreversible capacity losses in the first cycle and upon cycling has been carried out for two LNMO-based cathodes, one bare and one coated with ZnO. Galvanostatic tests performed at room and at 60 °C suggest that parasitic processes occur continuously upon cycling on the surface of LNMO-cathodes. In fact the cumulative irreversible capacity plots show an increasing trend even after 80 cycles. The ZnO coating confirms its ability to mitigate this effect. Impedance spectroscopy tests suggest the formation of a passivation film on the surface of the LNMO-based electrodes with an increasing resistance upon cycling.

Anodic LSV test shows that parasitic oxidations start on the surface of LNMO electrodes at potential slightly above the Ni^{2+}/Ni^{4+} redox couple. The ZnO coating is apparently able to broaden this process on a larger voltage range and to shift upwards the onset potential for this undesired reaction beyond 5 V. Ex situ TEM images recorded on charged electrodes highlight the precipitation of an uniform and continuous thin film (3–4 nm) on the bare LNMO particles upon first charge. However the formation of such thin and continuous film of the surface of the bare material does not

prevent the accumulation of further irreversible capacity losses upon cycling. The TEM images of the ZnO coated material shows rough surfaces without large alteration upon first charge.

The analysis of the coulombic efficiencies in the first cycle at various voltage cut-offs in GC tests suggest that irreversible capacity losses are suffered by the LNMO materials above 4.65 V vs. Li^+/Li. At lower voltages, although large in relative amounts, the irreversible charge loss is negligible. The major loss is observed at potential larger than 4.8 V. The ZnO coating does not alter drastically the overall picture but generally moderate the detrimental effects due to the electrolyte decomposition, in particular at cell potentials <4.65 V and >4.8 V vs. Li^+/Li. Impedance spectroscopy tests performed at various stages of charge and discharge upon the first galvanostatic cycle confirm the above described picture. In summary the evolution of the surface film resistance in the first cycle is qualitatively very similar for the bare and the coated LNMO materials. Upon charge the ZnO coating leads to a mitigation of the changes in the passivation film resistances. This effect can be put in direct relation with the mitigation of the parasitic reaction on the surface of the ZnO coated electrodes due to the HF trapping from the electrolyte.

Acknowledgments

The research leading to these results has received funding from the European Unions's 7th Framework Programme under grant agreement no. 265644 "Green Car".

One of the authors (S.B.) is grateful to the University of Rome Sapienza for a post-doctoral fellowship under the frame of the Project Ateneo 2010.

References

[1] R. Santhanam, B. Rambabu, Research progress in high voltage spinel $LiNi_{0.5}Mn_{1.5}O_4$ material, Journal of Power Sources 195 (2010) 5442.
[2] Y.K. Sun, K.J. Hong, J. Prakash, K. Amine, Electrochemical performance of nano-sized ZnO-coated $LiNi_{0.5}Mn_{1.5}O_4$ spinel as 5 V materials at elevated temperatures, Electrochemistry Communications 4 (2002) 344.
[3] K.M. Shaju, P.G. Bruce, Nano-$LiNi_{0.5}Mn_{1.5}O_4$ spinel: A high power electrode for Li-ion batteries, Dalton Transactions 40 (2008) 5471.
[4] J.C. Arrebola, A. Caballero, L. Hernan, J. Morales, Re-examining the effect of ZnO on nanosized 5 V $LiNi_{0.5}Mn_{1.5}O_4$ spinel: An effective procedure for enhancing its rate capability at room and high temperatures, Journal of Power Sources 195 (2010) 4278.
[5] D. Aurbach, B. Markovsky, G. Salitra, E. Markevich, Y. Talyossef, M. Koltypin, L. Nazar, B. Ellis, D. Kovacheva, Review on electrode-electrolyte solution interactions, related to cathode materials for Li-ion batteries, Journal of Power Sources 165 (2007) 491.
[6] Y. Talyosef, B. Markovsky, R. Lavi, G. Salitra, D. Aurbach, D. Kovacheva, M. Gorova, E. Zhecheva, R. Stoyanova, Comparing the behavior of nano- and micro-sized particles of $LiMn_{1.5}Ni_{0.5}O_4$ spinel as cathode materials for li-ion batteries, Journal of the Electrochemical Society 154 (2007) A682.
[7] H. Sclar, O. Haik, T. Menachem, J. Grinblat, N. Leifer, A. Meitav, S. Luski, D. Aurbach, The effect of ZnO and MgO coatings by a sono-chemical method, on the stability of $LiMn_{1.5}Ni_{0.5}O_4$ as a cathode material for 5 V li-ion batteries, Journal of the Electrochemical Society 159 (2012) A228.
[8] J. Mao, K. Dai, Y. Zhai, Electrochemical studies of spinel $LiNi_{0.5}Mn_{1.5}O_4$ cathodes with different particle morphologies, Electrochimica Acta 63 (2012) 381–390.
[9] L. Yang, B. Ravdel, B.L. Lucht, Electrolyte reactions with the surface of high voltage $LiNi_{0.5}Mn_{1.5}O_4$ cathodes for lithium-ion batteries, Electrochemical Solid-State Letters 13 (2010) A95.
[10] H. Duncan, Y. Abu-Lebdeh, I.J. Davidson, Study of the cathode-electrolyte interface of $LiMn_{1.5}Ni_{0.5}O_4$ synthesized by a sol-gel method for li-ion batteries, Journal of the Electrochemical Society 157 (2010) A528.
[11] S. Ivanova, E. Zhecheva, R. Stoyanova, D. Nihtianova, S. Wagner, P. Tzvetkova, S. Simova, High-voltage $LiNi_{1/2}Mn_{3/2}O_4$ spinel: Cationic order and particle size distribution, Journal of Physical Chemistry C 115 (2011) 25170.
[12] Z. Wang, N. Dupré, L. Lajaunie, P. Moreau, J.-F. Martin, L. Boutafa, S. Patoux, D. Guyomard, Effect of glutaric anhydride additive on the $LiNi_{0.4}Mn_{1.6}O_4$ electrode/electrolyte interface evolution: A MAS NMR and TEM/EELS study, Journal of Power Sources 215 (2012) 170.
[13] H. Duncan, D. Duguay, Y. Abu-Lebdeh, I.J. Davidson, Study of the $LiMn_{1.5}Ni_{0.5}O_4$ electrolyte interface at room temperature and 60 °C, Journal of the Electrochemical Society 158 (2011) A537.
[14] X. Wu, X. Li, Z. Wang, H. Guo, P. Yue, Capacity fading reason of $LiNi_{0.5}Mn_{1.5}O_4$ with commercial electrolyte, Ionics 19 (2013) 379.
[15] Y.K. Sun, Y.S. Lee, M. Yoshio, K. Amine, Synthesis and electrochemical properties of ZnO-coated $LiNi_{0.5}Mn_{1.5}O_4$ spinel as 5 V cathode material for lithium secondary batteries, Electrochemical Solid-State Letters 5 (2002) A99.
[16] Y.K. Sun, C.S. Yoon, I.H. Oh, Surface structural change of ZnO-coated $LiNi_{0.5}Mn_{1.5}O_4$ spinel as 5 V cathode materials at elevated temperatures, Electrochimica Acta 48 (2003) 503.
[17] L.H. Chi, N.N. Dinh, S. Brutti, B. Scrosati, Synthesis, characterization and electrochemical properties of 4.8 V $LiNi_{0.5}Mn_{1.5}O_4$ cathode material in lithium-ion batteries, Electrochimica Acta 55 (2010) 5110.
[18] S. Brutti, V. Gentili, P. Reale, L. Carbone, S. Panero, Mitigation of the irreversible capacity and electrolyte decomposition in a $LiNi_{0.5}Mn_{1.5}O_4$/nano-TiO_2 Li-ion battery, Journal of Power Sources 196 (2011) 9792–9799.
[19] M.D. Abramoff, P.J. Magalhaes, S.J. Ram, Image processing with imageJ, Biophotonics International 11 (2004) 36–42.
[20] W.S. Rasband, ImageJ, U.S. National Institutes of Health, Bethesda, MD, USA, 1997–2011 http://imagej.nih.gov/ij/
[21] Ü. Özgür, YaI. Alivov, C. Liu, A. Teke, M.A. Reshchikov, S. Doğan, V. Avrutin, S.-J. Cho, A comprehensive review of ZnO materials and devices, Journal of Applied Physics 98 (2005) 041301.
[22] D. Aurbach, M.D. Levi, E. Levi, H. Teller, B. Markovsky, G. Salitra, U. Heider, L. Heider, Common electroanalytical behavior of Li intercalation processes into graphite and transition metal oxides, Journal of the Electrochemical Society 145 (1998) 3024.
[23] N. Marandian Hagh, F. Cosandey, S. Rangan, R. Bertynski, G.G. Amatucci, Electrochemical performance of acid-treated nanostructured $LiMn_{1.5}Ni_{0.5}O_4$-δ spinel at elevated temperature, Journal of the Electrochemical Society 157 (2010) A305.
[24] T. Ohsaki, T. Kishi, T. Kuboki, N. Takami, N. Shimura, Y. Sato, M. Sekino, A. Satoh, Overcharge reaction of lithium-ion batteries, Journal of Power Sources 146 (2005) 97–100.